Eur Biophys J (2012) 41:561–570
DOI 10.1007/s00249-012-0818-4

ORIGINAL PAPER

EBSA
Biophysics in Europe

Contour and persistence length of *Corynebacterium diphtheriae* pili by atomic force microscopy

Johannes Rheinlaender · Anna Gräbner · Lisa Ott · Andreas Burkovski · Tilman E. Schäffer

Received: 10 January 2012 / Revised: 5 April 2012 / Accepted: 21 April 2012 / Published online: 16 May 2012

Abstract Many bacteria are characterized by nanoscale ultrastructures, for example S-layers, flagella, fimbriae, or pili. The last two are especially important for attachment to different abiotic and biotic surfaces and for host–pathogen interactions. In this study, we investigated the geometric and elastic properties of pili of different *Corynebacterium diphtheriae* strains by atomic force microscopy (AFM). We performed quantitative contour-length analysis of bacterial pili and found that the visible contour length of the pili can be described by a log-normal distribution. Our data revealed significant strain-specific variations in the mean visible contour length of the pili, ranging from 260 to 1,590 nm. To estimate their full contour length, which is not directly accessible from the AFM images, we developed a simple correction model. Using this model, we determined the mean full contour length as 510–2,060 nm. To obtain the persistence length we used two different methods of analysis, one based on the end-to-end distance of the pili and one based on the bending angles of short segments. In comparison, the bending angle analysis proved to be more precise and resulted in persistence lengths in the narrow range of 220–280 nm, with no significant strain-specific variations. This is small compared with some other bacterial polymers, for example type IV pili, F-pili, or flagella.

Keywords Bacteria · AFM · Contour length · Persistence length · Stiffness

Electronic supplementary material The online version of this article (doi:10.1007/s00249-012-0818-4) contains supplementary material, which is available to authorized users.

J. Rheinlaender · A. Gräbner · T. E. Schäffer
Institute of Applied Physics, University of Erlangen-Nuremberg, Erlangen, Germany

L. Ott · A. Burkovski
Chair for Microbiology, University of Erlangen-Nuremberg, Erlangen, Germany

Present Address:
T. E. Schäffer (✉)
Institute of Applied Physics, University of Tübingen, Auf der Morgenstelle 10, 72076 Tübingen, Germany
e-mail: Tilman.Schaeffer@uni-tuebingen.de

Introduction

The first crucial steps of interaction of pathogens with their corresponding hosts are host recognition and binding to the host's surface. For this purpose, many bacteria possess fimbriae and pili, which facilitate attachment to different abiotic and biotic surfaces.

Corynebacterium diphtheriae is the etiological agent of diphtheria, a localized infection of the upper respiratory tract and skin (cutaneous diphtheria), which can be fatal, because of the potent diphtheria toxin. Adhesion of different *C. diphtheriae* strains to lung, pharyngeal, and laryngeal epithelial cells and to erythrocytes has been reported (Colombo et al. 2001; Bertuccini et al. 2004; Hirata et al. 2002, 2004). Although it is known that both cell-wall-linked surface proteins and fibrous protein polymers, for example fimbriae and pili, are of major importance in the adhesion process for many types of Gram-positive bacteria, many aspects of the underlying mechanisms remain unclear (Rogers et al. 2011). For *C. diphtheriae* the effect of pili on recognition of and adhesion to host cells have recently been characterized on the genetic level. Analysis of mutants has revealed that *C. diphtheriae* type strain NCTC13129 is able to assemble pili from different pilin subunits on its surface. Pili are

important for bacterium–host cell contact and host cell preference (Gaspar and Ton-That 2006; Swierczynski and Ton-That 2006; Mandlik et al. 2007), making them an interesting focus of research to understand host–pathogen interaction. Recently, it has been reported that the expression of different pilin subunit proteins in *C. diphtheriae* affects pili length qualitatively (Swierczynski and Ton-That 2006; Mandlik et al. 2008; Guttilla et al. 2009). However, a comprehensive statistical analysis of the pili, e.g. giving the mean contour length, has not yet been reported for *C. diphtheriae*. Also, the persistence length, which is an important measure of the mechanical stiffness of filamentous polymers, has not yet been reported for *C. diphtheriae* pili.

Pili and other bacterial cell appendices and surface structures are often studied by electron microscopy, which requires staining or labeling procedures. Atomic force microscopy (AFM) can image the topography of unstained samples and has already been intensively applied to the study of bacteria (Anselmetti et al. 2007; Dupres et al. 2009; Wright et al. 2010) and to bacterial pili (Touhami et al. 2006; Miller et al. 2006; Fälker et al. 2008; Arce et al. 2009). The contour length of the pili can vary by one order of magnitude within a single cell (Yanagawa and Honda 1976; Touhami et al. 2006). However, when imaged while being attached to the cell body, the contour length of the pili can be systematically underestimated.

Here we describe comprehensive characterization of pili ultrastructure for five different *C. diphtheriae* strains, giving two important quantities: the mean full contour length and the persistence length. For this purpose, we develop a simple model for estimating the mean full contour length from the experimentally accessible mean visible contour length in high resolution microscopy images. To obtain persistence length of the pili we used two different analysis methods: one based on the end-to-end distance and one based on the bending angles of short pili segments. Finally, we relate the strain-specific variations in pili formation to the different abilities for adhesion and invasion of host cells found in previous studies and to genetic information (Swierczynski and Ton-That 2006; Mandlik et al. 2007; Guttilla et al. 2009; Ott et al. 2010).

Methods

Growth of bacteria and sample preparation

Corynebacterium diphtheriae overnight cultures grown in 20 ml HI broth were washed five times in 20 ml ice-cold distilled water and were resuspended in 10 ml ice-cold distilled water. Five microliters of each sample was fixed on a glass slide or freshly cleaved mica substrate by drying, by use of compressed air.

Atomic force microscopy

The samples were imaged by AFM (MFP-3D; Asylum Research, Santa Barbara, USA) using standard silicon cantilever probes (NCH-W; Nanosensors, Neuchatel, Switzerland) in tapping mode under ambient laboratory conditions. All images are unprocessed except for line-by-line polynomial background removal ("flattening"). All data analysis was performed in IgorPro (Wavemetrics, Lake Oswego, OR, USA) by use of custom-written software and least-squares fitting routines.

Theoretical background

Persistence length

To determine the persistence length of the pili, we used the worm-like chain (WLC) model, which describes a semi-flexible polymer chain in thermodynamic equilibrium (Landau et al. 1980). The WLC model has been applied to many filamentous biomolecules and biostructures, for example actin (Nagashima and Asakura 1980; Yanagida et al. 1984), microtubules (Gittes et al. 1993), DNA (Rivetti et al. 1996), bacterial flagella (Trachtenberg and Hammel 1992), type F-pili (Silverman and Clarke 2010), and type IV pili (Skerker and Berg 2001). In this model, the polymer is described as a homogenous elastic rod with a circular cross-section. The energy U required to bend a polymer segment of length ΔL by an angle ϑ is given by:

$$U(\vartheta) = \frac{EI}{2\Delta L}\vartheta^2, \tag{1}$$

where E is the stiffness (Young's modulus) and $I = \pi r^4/4$ is the polymer's cross sectional area moment of inertia, where r is the radius of the cross section (Landau et al. 1986). In thermodynamic equilibrium, the probability p that the segment is bent by a specific angle is given by Boltzmann's law:

$$p(\vartheta) \propto e^{-\frac{U(\vartheta)}{k_B T}} = e^{-\frac{1}{2}\frac{P}{\Delta L}\vartheta^2}. \tag{2}$$

Consequently, the standard deviation σ_ϑ of the bending angles is given by $\sigma_\vartheta^2 = \langle\vartheta^2\rangle = \Delta L/P$ and the moments of the bending angle distribution fulfill $\langle\vartheta^4\rangle/\langle\vartheta^2\rangle^2 = 3$. The persistence length of the polymer:

$$P = \frac{EI}{k_B T}, \tag{3}$$

can be interpreted as the distance along the polymer at which its angular orientation becomes uncorrelated. For a long polymer of contour length L that is confined within a plane, the WLC model predicts the mean squared end-to-end distance as (Rivetti et al. 1996):

$$\langle R^2 \rangle = 4PL\left[1 - \frac{2P}{L}\left(1 - e^{-\frac{L}{2P}}\right)\right]. \quad (4)$$

Log-normal distribution

Growth processes with randomly fluctuating growth rates often have log-normal distributions (Koch 1966). Hence, many quantities in biology, but also in many other fields, for example medicine, social sciences, and economics, are log-normally distributed (Limpert et al. 2001). For a log-normally distributed random variable L, the variable's natural logarithm $x = \ln(L)$ is normally distributed. So the probability density function ϕ for x is:

$$\phi_{\mu,\sigma}(x) = \frac{1}{\sqrt{2\pi}\sigma}\exp\left(-\frac{(x-\mu)^2}{2\sigma^2}\right), \quad (5)$$

where μ and σ are the arithmetic mean and the standard deviation, respectively, of the distribution. Consequently, the probability density function of L is:

$$f(L) = \phi_{\mu,\sigma}(x)\frac{\mathrm{d}x}{\mathrm{d}L} = \frac{1}{\sqrt{2\pi}\sigma L}\exp\left(-\frac{(\ln(L)-\mu)^2}{2\sigma^2}\right) \quad (6)$$

and the cumulative distribution function is:

$$F(L) = \int_0^L f(L')\,\mathrm{d}L' = \int_{-\infty}^{\ln(L)} \phi_{\mu,\sigma}(x')\,\mathrm{d}x' = \frac{1}{2}\mathrm{erfc}\left(-\frac{\ln(L)-\mu}{\sqrt{2}\sigma}\right). \quad (7)$$

Here, "erfc" denotes the complementary error function.

For a log-normal distribution the geometric mean $\bar{L}$ is related to the arithmetic mean μ of x by $\bar{L} = \exp(\mu)$. The standard deviation of x, σ, can be transformed to the geometric standard deviation of L, $\sigma_{\mathrm{GSD}} = \exp(\sigma)$. For the normally distributed x the interval $\mu \pm \sigma$ ranges from $\mu - \sigma$ to $\mu + \sigma$ and covers approximately 68.3 % of the data. For the log-normally distributed L the corresponding interval $\exp(\mu \pm \sigma)$ ranges from $\bar{L}/\sigma_{\mathrm{GSD}}$ to $\bar{L} \times \sigma_{\mathrm{GSD}}$. The 95 % confidence interval of the mean after N measurements, which ranges from $\mu - t \times \sigma/\sqrt{N}$ to $\mu + t \times \sigma/\sqrt{N}$ for a normally distributed x, is transformed accordingly, resulting in a range from $\bar{L}/\exp[t \times \sigma/\sqrt{N}]$ to $\bar{L} \times \exp[t \times \sigma/\sqrt{N}]$ for a log-normally distributed L. The expression $t = t_{0.975,N-1}$ denotes the 97.5th percentile of the Student's t-distribution with $N - 1$ degrees of freedom.

Experimental results

Characterization of the ultrastructure of pili

AFM topography images of *C. diphtheriae* strains revealed pili on the substrate extending from the cell bodies (Fig. 1a–e, arrows). Strain-specific differences in pili number and morphology were apparent. For example, whereas DSM44123 cells had only a small number of sub-micrometer long, relatively straight pili (Fig. 1b), ISS4749 cells had many pili, which were much longer and at first sight seemed more curved (Fig. 1e). DSM43988 cells had no pili (Fig. 1f).

To obtain quantitative, strain-specific differences among length and curvature, we performed a systematic study of the pili. First, we recorded many images of pili for the different strains at high resolution. In offline analysis, we then manually traced the pili by selecting close-spaced points along their contour (Fig. 2a). Only pili that were clearly identifiable along their entire contour on the substrate and with a visible length of at least 100 nm were selected for analysis. Sufficient statistical precision was achieved by analyzing approximately 30 individual pili for each strain which originated from 6 to 17 different cells. To investigate the effect of the substrate on persistence length, cells prepared on both glass and mica were analyzed. Finally, we converted the sets of points into smooth contour paths by cubic spline interpolation (Fig. 2b). Interpolation was necessary because contour length estimation of a curved structure from a discrete set of points can lead to significant discrepancies between actual and determined contour length (Dorst and Smeulders 1987). These discrepancies can be reduced to less than 1 % by cubic spline interpolation, as was demonstrated for AFM images of DNA molecules (Rivetti and Codeluppi 2000).

We also estimated the diameters of the pili by analyzing their cross sections in the high-resolution AFM images; they were 1–2 nm for all strains.

Visible contour length

As is apparent in the AFM images (Fig. 1), the visible contour length of the pili for a given *C. diphtheriae* strain varies. We therefore statistically analyzed the measured visible contour lengths L of the imaged pili by generating a cumulative histogram for each strain (Fig. 3a, b, and Suppl. Fig. S1, black curves). The log-normal distribution describes the data well, as can be seen by the close match between the measured cumulative histograms and the corresponding cumulative distribution functions, using the respective $\bar{L}$ and σ_{GSD} of the data (solid gray curves). More formally, we confirmed this close match by a

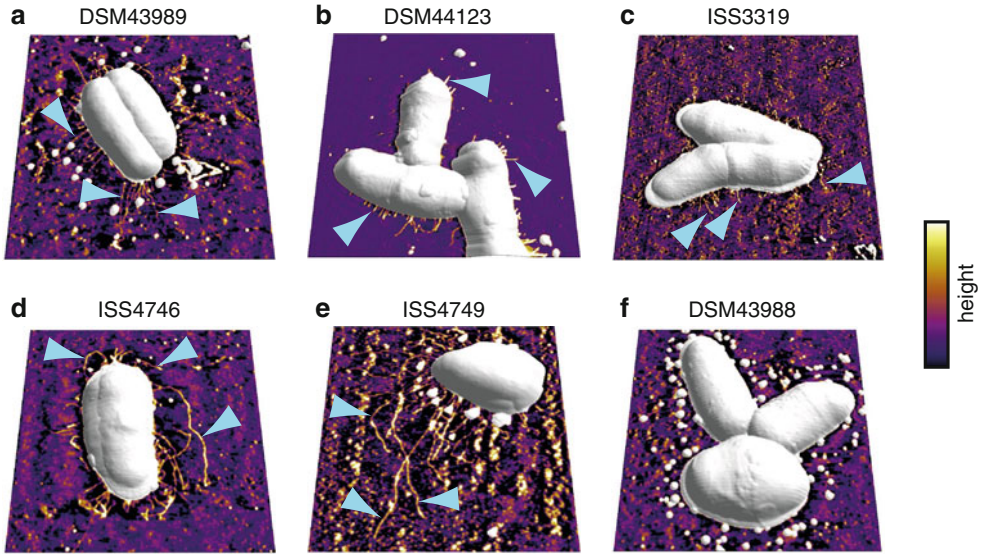

Fig. 1 **a–f** AFM topography images of bacteria from different *C. diphtheriae* strains. Pili of different number, length, and curvature appear as fine lines extending from the cell bodies (*blue arrows*). For example, DSM44123 cells (**b**) have only a small number of sub-micrometer long pili, whereas ISS4749 cells (**e**) have many pili up to several micrometers long. DSM43988 cells (**f**) do not have pili. Scan size 4 μm × 4 μm, height data range 500 nm, color scale range 2 nm

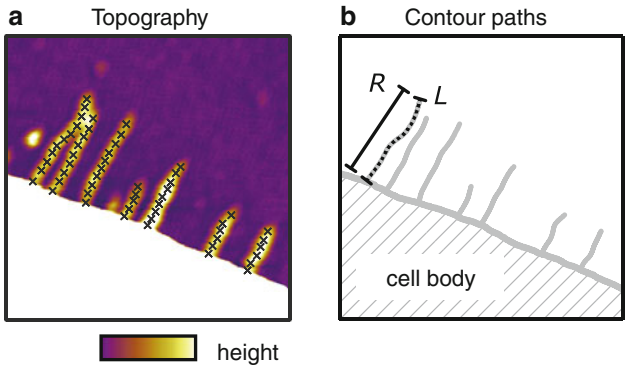

Fig. 2 Analysis of pili ultrastructure. **a** High-resolution AFM topography image of the edge of a DSM44123 cell. Pili contours were traced by manually selecting several points along each pilus (markers). Only pili that were clearly identifiable along their entire contour on the substrate and with a visible length of at least 100 nm were selected for analysis. **b** A smooth contour path was generated from selected points along each pilus by cubic spline interpolation, enabling an accurate determination of the visible contour length L and the visible end-to-end distance R. Scan size 500 nm × 500 nm, color scale range 2 nm

Kolmogorow–Smirnow test using a significance level $\alpha = 0.05$. This justifies the use of the log-normal distribution.

The results for the mean visible contour lengths for the different strains are plotted in Fig. 3c and are listed in Table 1. The differences between the mean visible contour lengths for the five strains were statistically significant as confirmed by Student's t tests applied to the logarithmically transformed data (Limpert and Stahel 2011; p values < 0.01), except for the difference between DSM43989 and ISS4746 (p value $= 0.025$) and the difference between DSM44123 and ISS3319 (p value $= 0.083$).

Full contour length

The pili in the AFM images could be identified on the substrate but not on the cell bodies, owing to the relatively large surface roughness (several nanometers) of the cell bodies. Therefore, the full contour length of a pilus is longer than its visible contour length by the part that lies on the cell body (Fig. 3d). The consequence is that the measured, visible contour lengths (Fig. 3c and Table 1) underestimate the respective full contour lengths. To estimate the full contour lengths we developed a simple, one-dimensional model using four simplifications.

1. Because *C. diphtheriae* cells are rod-shaped and elongated the statistical effect of the pili at the cell poles is small. We therefore excluded them from the model.
2. A pilus is anchored in the cell surface at a random position.
3. Because the persistence length is similar in size to the width of the body of a typical cell, the pili were modeled as straight.
4. For simplicity we assumed the pili were of equal length for each strain and were oriented perpendicular to the long cell axis.

We now consider the two limiting cases:

1. short pili with a full contour length smaller than the upper perimeter B of the cell body (Fig. 4a); and
2. long pili with a full contour length larger than the upper perimeter B of the cell body (Fig. 4b).

For the short pili, some of the pili reach the substrate and become visible. On average their visible contour length is half their full length: $\bar{L} \approx \bar{L}_{\text{full}}/2$. For long pili all pili reach the substrate and, on average, the visible contour length

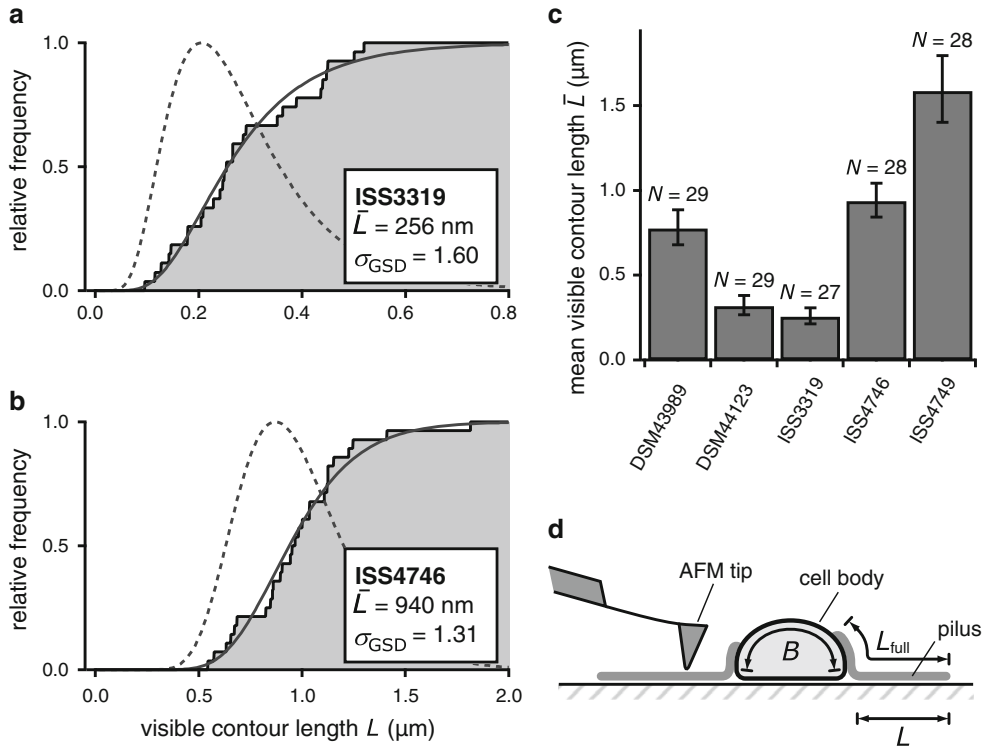

Fig. 3 Contour length analysis. **a**, **b** Cumulative histograms of measured visible contour lengths of pili **a** from strain ISS3319 and **b** from strain ISS4746 (*black curves*) with respective geometric means $\bar{L}$ and geometric standard deviations σ_{GSD}. The corresponding log-normal cumulative distribution functions (Eq. 7) (*solid gray curves*) match the experimental data well. Also shown are the corresponding probability density functions (Eq. 6) (not normalized) (*dashed gray curves*). The cumulative histograms for the remaining strains are shown in Suppl. Fig. S1. **c** Strain-specific visible contour lengths (geometric mean, *error bars* represent the 95 % confidence intervals). Statistical significance of the differences (Student's *t* test): *p* value < 0.01 for all pairs except for the pair DSM43989—ISS4746 (*p* value $= 0.025$) and the pair DSM44123—ISS3319 (*p* value $= 0.083$). **d** Schematic diagram illustrating the difference between the visible (L) and the full (L_{full}) contour length of a pilus. *B* denotes the upper perimeter of the cell body

Table 1 Measured mean visible contour length (geometric mean $\bar{L}$), mean full contour length from the correction model, and persistence length from method 2 (segment bending angles) for the pili from five different *C. diphtheriae* strains

Strain	Mean visible contour length (nm)	Mean full contour length (nm)	Persistence length (nm) (method 2)
DSM43989	780 [680, 880]	1,230 [1,070, 1,400]	220 [190, 250]
DSM44123	320 [270, 380]	640 [530, 760]	280 [230, 340]
ISS3319	260 [210, 310]	510 [430, 620]	280 [220, 350]
ISS4746	940 [840, 1,040]	1,390 [1,250, 1,540]	240 [210, 270]
ISS4749	1,590 [1,400, 1,790]	2,040 [1,800, 2,300]	260 [230, 280]

The values in parentheses indicate the respective 95 % confidence interval

differs from the full contour length by half of the upper perimeter of the cell body: $\bar{L}_{full} - \bar{L} \approx B/2$. In summary, the mean full contour length can be approximated from the mean visible contour length by:

$$\bar{L}_{full} \approx \bar{L} + \begin{cases} \bar{L}; & \bar{L} < B/2 \\ B/2; & \bar{L} \geq B/2 \end{cases}. \quad (8)$$

Here we used $B = 1$ µm as a typical upper perimeter of the cell body for all strains analyzed. The results of the correction based on Eq. (8) are shown in Fig. 4c and Table 1.

Persistence length

To obtain the persistence length P of the pili we used two different methods of analysis. The first method is based on the end-to-end distance ("method 1") and has previously been applied to biopolymers such as DNA (Rivetti et al. 1996; Mantelli et al. 2011), flagella (Trachtenberg and Hammel 1992), F-pili (Silverman and Clarke 2010), and filamentous bacteriophages (Wang et al. 2006). Using this method we plotted, for each strain, the mean squared

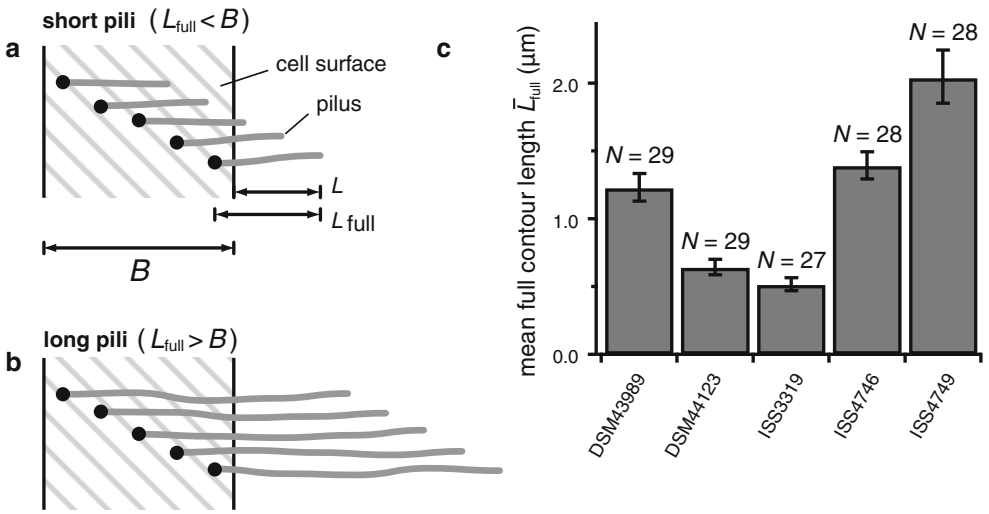

Fig. 4 One-dimensional model for estimating the mean full contour length of the pili. **a** Short pili with a full contour length $\bar{L}_{full}$ smaller than the upper perimeter B of the cell body. Only some of the pili reach the substrate and become visible in the AFM images. On average their visible contour length is half their full contour length: $\bar{L} \approx \bar{L}_{full}/2$. **b** Long pili with a full contour length $\bar{L}_{full}$ larger than the upper perimeter B of the cell body. All pili reach the substrate and on average the visible contour length differs from the full contour length by half of the upper perimeter B: $\bar{L}_{full} - \bar{L} \approx B/2$. **c** Strain-specific mean full contour lengths (geometric mean, *error bars* indicate the 95 % confidence intervals)

visible end-to-end distance R^2 of each pilus vs. its visible contour length L. This is shown in Fig. 5a for strain DSM44123 as an example; the measured values of R^2 and L are labeled with different markers for a preparation on a glass ("+") or mica ("×") as substrate. We then fitted Eq. (4) to these data (Fig. 5a, solid line) to obtain the persistence length P of the pili. For strain DSM44123, using method 1, we obtained $P = 520 \pm 160$ nm (fit coefficient ±95 % confidence interval). The persistence lengths of the other strains were obtained similarly (for the other strains see Suppl. Fig. S2). The resulting persistence lengths based on the end-to-end distance range from 280 to 520 nm and are plotted in Fig. 5b.

However, two problems arise from this method when applied to polymers of different contour length: first, long polymers have an overly high effect on the fit and hence on the resulting persistence length. Second, the width of the confidence interval obtained is only a lower estimate, because the statistical fluctuation of R^2 is not included. Furthermore, because only one value per polymer (the end-to-end distance) is measured the statistical sample is relatively small. As can be seen in Fig. 5b the differences obtained between strain-specific persistence lengths are high (approx. a factor of two), nevertheless they are not statistically significant (Student's t tests give p values > 0.01 for all pairs).

To improve the statistical precision we therefore applied a second method that is based on the bending angle of short polymer segments ("method 2"). This was possible because the paths of the pili were traced digitally. Similar methods have been applied to DNA (Bednar et al. 1995; Abels et al. 2005), for which the statistics of the cosine of the bending angle, $\cos(\vartheta)$, were considered. However, as can be seen from Eq. (2), the persistence length can also be directly obtained from the standard deviation of the bending angles, σ_ϑ. This has particular benefits compared with method 1:

- first, because much more information is used, the statistical precision is much higher for the same number of polymers; and
- second, the statistical uncertainty follows directly from the statistics of the standard deviation.

The 95 % confidence interval of σ_ϑ^2 after measuring N_s polymer segments is given by:

$$\left[\frac{N_s - 1}{\chi^2_{N_s-1,0.975}} s_\vartheta^2, \quad \frac{N_s - 1}{\chi^2_{N_s-1,0.025}} s_\vartheta^2\right]. \tag{9}$$

Therefore, the 95 % confidence interval of the resulting persistence length P is:

$$\left[\frac{\Delta L}{s_\vartheta^2} \frac{\chi^2_{N_s-1,0.025}}{N_s - 1}, \quad \frac{\Delta L}{s_\vartheta^2} \frac{\chi^2_{N_s-1,0.975}}{N_s - 1}\right]. \tag{10}$$

Here, s_ϑ^2 is the measured sample variance of the bending angle, $\chi^2_{N_s-1,0.025}$ and $\chi^2_{N_s-1,0.975}$ denote the 2.5th and 97.5th percentiles of the chi-squared distribution with $N_s - 1$ degrees of freedom.

Figure 5c shows the histogram of bending angles using pili segments of length $\Delta L = 50$ nm for strain DSM44123 as an example (for the other strains see Suppl. Fig. S3). The mean bending angle is zero within

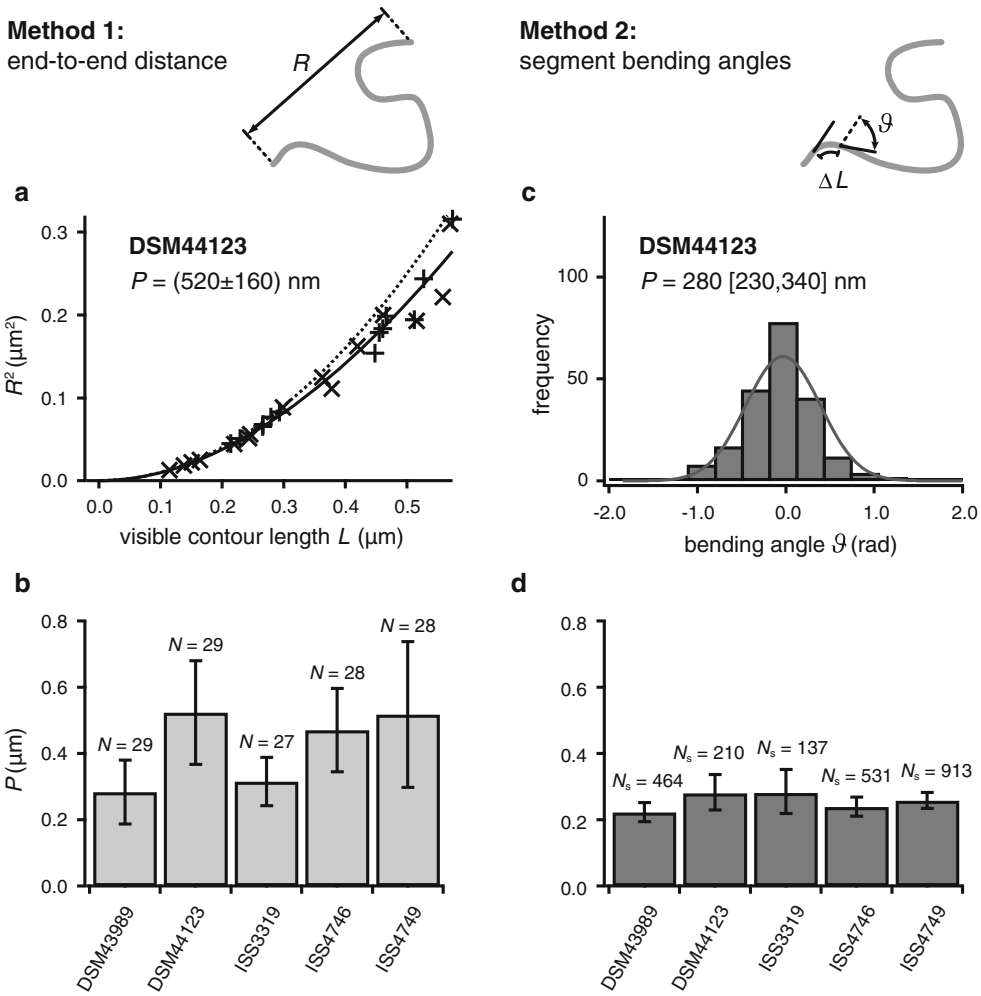

Fig. 5 Two methods for persistence length analysis, both shown for strain DSM44123 as example (for the other strains see Suppl. Figs. S2 and S3). **a** *Method 1*: Squared visible end-to-end distance R^2 versus visible contour length L. The persistence length P (±95 % confidence interval) is determined by fitting Eq. (4) (*solid line*). The *dotted line* indicates the limit of infinitely stiff pili, corresponding to $R^2 = L^2$. *Different markers* represent preparations on glass (*plus*) or mica (*cross*) as substrates. **b** Strain-specific persistence lengths based on R^2 versus L data. **c** *Method 2*: Histogram of bending angles using segments of length $\Delta L = 50$ nm. The standard deviation of the bending angles $\sigma_\vartheta = 0.42$ [0.35, 0.52] corresponds to a persistence length of $P = 280$ [230, 340] nm. The *gray trace* shows the corresponding Gaussian distribution from Eq. (2). **d** Strain-specific persistence lengths based on the segment bending angles. *Error bars* indicate the 95 % confidence intervals

the measurement precision, $\langle\vartheta\rangle = -0.03$ [−0.09, 0.03], and the standard deviation of the bending angles is $\sigma_\vartheta = 0.42$ [0.35, 0.52]. The values in brackets indicate the corresponding 95 % confidence intervals based on Eq. (9). Furthermore, the distribution is Gaussian, as indicated by the close match with the corresponding distribution from Eq. (2) (gray trace) (for the other strains see Suppl. Fig. S3). The standard deviation of the bending angles corresponds to a persistence length of $P = \Delta L/\sigma_\vartheta^2 = 280$ [230, 340] nm. The persistence lengths based on the bending angle statistics (method 2) are summarized in Fig. 5d and are listed in Table 1. It can be seen that the strain-specific persistence lengths from method 2 are within a narrow range of 220–280 nm and that the confidence intervals are much smaller than those for method 1. Nevertheless, the differences between the persistence lengths from the different strains are still not significant (Student's t tests give p values > 0.05 for all pairs). When we applied method 2 to the data from the preparations on glass and mica separately, no significant effect of the substrate on the measured persistence length was detected.

Discussion

Pili are crucial for adhesion to host cells, and for different *C. diphtheriae* strains this process varies substantially (Ott et al. 2010). Surprisingly, there seems to be no direct correlation between adhesion efficiency and pili number or length. Whereas ISS4746 and ISS4749 have long pili (Fig. 3c) and strong adhesion, DSM43989 has long pili but adheres much less strongly, and DSM44123 and ISS3319 have short pili but moderate adhesion.

One important question is whether features of the bacterial phenotype, for example pili contour length, can be related to genetic information. Pili subunits SpaA and SpaH have been identified as the main shaft proteins of *C. diphtheriae*, and their existence or overproduction have been found to increase the pili contour length (Swierczynski and Ton-That 2006; Mandlik et al. 2007; Guttilla et al. 2009). Strains ISS4746 and ISS4749 have a large pili contour length (Fig. 3c) and high expression of SpaA and SpaH (Ott et al. 2010). On the other hand, strains DSM44123 and ISS3319, which have short pili, and express no SpaH and comparatively little SpaA. Therefore,

increased expression of SpaA and SpaH in combination or alone might result in increased pili length.

To analyze the mechanical properties of the pili, we applied the WLC model to determine the persistence length. We used two different methods of analysis, based on the end-to-end distance (method 1, Fig. 5b) and on the bending angles of short segments (method 2, Fig. 5d). In comparison, two differences can be seen between the persistence lengths when using method 1 and when using method 2.

- First, the confidence intervals from method 2 are smaller than those from method 1.
- Second, on average, the persistence lengths from method 2 seem to be smaller.

There are three main reasons for these differences.

- First, in method 1 only one value per pili is used. The statistical sample of approximately 30 pili per strain is therefore much smaller than for method 2 in which approximately 100–900 segments per strain are analyzed.
- Second, because the persistence length is positive by definition, noise will, on average, increase the resulting persistence length.
- Third, method 1 is more sensitive to directional bias.

These reasons imply that method 2 is both more accurate and more precise. Therefore, we only consider the results from method 2 (Table 1) in the following discussion.

By estimating statistical error we found that differences in persistence length between the strains were not significant (Student's t test p values > 0.05). In general, the persistence length of *C. diphtheriae* pili seems to be significantly lower than the persistence lengths of other bacterial polymers, for example type IV pili ($P \approx 5$ μm; Skerker and Berg 2001), F-pili ($P \approx 5$ μm; Silverman and Clarke 2010), or bacterial flagella ($P \approx 20$–40 μm; Trachtenberg and Hammel 1992). *C. diphtheriae* pili are also much more flexible than actin ($P \approx 20$ μm) or microtubules ($P \approx 5$ mm; Gittes et al. 1993), but they are stiff in comparison with DNA ($P \approx 50$ nm; Taylor and Hagerman 1990; Rivetti et al. 1996). Interestingly, the persistence length of filamentous bacteriophages ($P \approx 1$ μm) is similar to that of *C. diphtheriae* pili (Wang et al. 2006).

One limitation possibly affecting our measurements and those previously obtained by electron microscopy is the use of dried samples. It is known for electrically charged polymers, for example DNA, that changing local electrostatic interactions have an effect on persistence length (Baumann et al. 1997; Mantelli et al. 2011). *C. diphtheriae* pili, however, are probably uncharged (Kang et al. 2009), making the persistence length of the pili insensitive to electrostatic conditions. Another possible limitation of our analysis is the assumption that the pili thermally equilibrate in the substrate plane (Eq. 4) before they are immobilized by the drying process (Wang et al. 2006; Silverman and Clarke 2010). This is in contrast with another possible scenario in which the pili are "kinetically trapped" on the substrate, i.e. are immobilized immediately upon initial contact with the substrate. For polymers without a charge or with a low charge, for example *C. diphtheriae* pili, however, this scenario is less likely (Bezanilla et al. 1995).

From the AFM images we estimated the diameter of the pili as 1–2 nm. This is smaller than the value obtained by electron microscopy (2.5–3.5 nm; Yanagawa and Honda 1976). A possible explanation of this discrepancy is that AFM might underestimate the diameter because of the non-zero imaging force that indents soft samples (Jiao and Schäffer 2004). Electron microscopy, on the other hand, might overestimate the diameter because of the conductive coating required before imaging. From the crystal structure of the pili subunit SpaA (Kang et al. 2009), we read off a diameter of 2.5 nm. In the following discussion, we assume a diameter of 2.5 nm to estimate the stiffness of the pili.

In combination with the persistence length, the pili diameter can be used to estimate the stiffness (Young's modulus) of the pili by rearranging Eq. (3) and assuming the pili are homogeneous, isotropic cylindrical rods of diameter 2.5 nm. This gives a stiffness of 400–600 MPa for the analyzed *C. diphtheriae* strains. In general, the stiffness of *C. diphtheriae* pili is greater than that of DNA, which is approximately 100–300 MPa, depending on base composition (Hogan et al. 1983) and on the composition (Wang et al. 1997) and ionic strength (Baumann et al. 1997) of the surrounding buffer solution. But it is smaller than that of some other proteins, for example microtubules ($E \approx 1.2$ GPa; Gittes et al. 1993) or actin filaments ($E \approx 2$ GPa; Kojima et al. 1994; Huxley et al. 1994). It is also smaller than that of electrically conductive microbial nanowire pili ($E \approx 1$ GPa; Leung et al. 2011), which were discovered recently (Reguera et al. 2005).

Our results also enable us to draw conclusions about the mechanical properties of the pili subunits. The pili of strains ISS4746 und ISS4749 consist of SpaA and SpaH subunits whereas the pili of the other strains in this study consist of SpaH only (Ott et al. 2010). Because the pili persistence lengths of all investigated strains were similar (within the precision of our measurement), we can conclude that SpaA and SpaH must contribute approximately equally to the persistence length.

Conclusion

We have performed comprehensive AFM analysis of pili contour length and persistence length for different

C. diphtheriae strains. Measurements revealed significant strain-specific differences among mean visible contour length. Because each pilus lay partially on the cell body, on which it could not be visualized, its visible contour length underestimated its full contour length. By use of a simple model we estimated mean full contour lengths for the different strains as 510–2,060 nm, with significant strain-specific variation. We also measured the persistence lengths of the pili—as far as we are aware the first such analysis for type III pili. We used two different methods of analysis—one based on the end-to-end distance and one based on the bending angles of short segments. The bending angle analysis proved to be more precise. The persistence lengths did not vary significantly among the strains investigated, and were in the range 220–280 nm, which is relatively low compared with other bacterial polymers, for example type IV pili, F-pili, or flagella.

Acknowledgments ISS strains were kindly provided by C. v. Hunolstein (Istituto Superiore di Sanita, Rome). LO and AB are grateful for financial support of the *Deutsche Forschungsgemeinschaft* (SFB796, B5). We thank Yves Muller (Biotechnology Division, University of Erlangen-Nuremberg) for assistance with the Protein Data Bank. We thank Asylum Research and Atomic Force F&E for support.

References

Abels JA, Moreno-Herrero F, van der Heijden T, Dekker C, Dekker NH (2005) Single-molecule measurements of the persistence length of double-stranded RNA. Biophys J 88(4):2737–2744. doi:10.1529/biophysj.104.052811

Anselmetti D, Hansmeier N, Kalinowski J, Martini J, Merkle T, Palmisano R, Ros R, Schmied K, Sischka A, Toensing K (2007) Analysis of subcellular surface structure, function and dynamics. Anal Bioanal Chem 387(1):83–89. doi:10.1007/s00216-006-0789-3

Arce FT, Carlson R, Monds J, Veeh R, Hu FZ, Stewart PS, Lal R, Ehrlich GD, Avci R (2009) Nanoscale structural and mechanical properties of nontypeable *Haemophilus influenzae* biofilms. J Bacteriol 191(8):2512–2520. doi:10.1128/jb.01596-08

Baumann CG, Smith SB, Bloomfield VA, Bustamante C (1997) Ionic effects on the elasticity of single DNA molecules. Proc Natl Acad Sci USA 94(12):6185–6190

Bednar J, Furrer P, Katritch V, Stasiak A, Dubochet J, Stasiak A (1995) Determination of DNA persistence length by cryo-electron microscopy. Separation of the static and dynamic contributions to the apparent persistence length of DNA. J Mol Biol 254(4):579–594. doi:10.1006/jmbi.1995.0640

Bertuccini L, Baldassarri L, von Hunolstein C (2004) Internalization of non-toxigenic *Corynebacterium diphtheriae* by cultured human respiratory epithelial cells. Microb Pathog 37(3):111–118. doi:10.1016/j.micpath.2004.06.002

Bezanilla M, Manne S, Laney DE, Lyubchenko YL, Hansma HG (1995) Adsorption of DNA to mica, silylated mica, and minerals: characterization by atomic force microscopy. Langmuir 11(2):655–659. doi:10.1021/la00002a050

Colombo AV, Hirata R Jr, de Souza CM, Monteiro-Leal LH, Previato JO, Formiga LC, Andrade AF, Mattos-Guaraldi AL (2001) *Corynebacterium diphtheriae* surface proteins as adhesins to human erythrocytes. FEMS Microbiol Lett 197(2):235–239. doi:10.1111/j.1574-6968.2001.tb10609.x

Dorst L, Smeulders AWM (1987) Length estimators for digitized contours. Comput Vis Graph Image Process 40(3):311–333

Dupres V, Alsteens D, Pauwels K, Dufrêne YF (2009) In vivo imaging of S-layer nanoarrays on *Corynebacterium glutamicum*. Langmuir 25(17):9653–9655. doi:10.1021/la902238q

Fälker S, Nelson AL, Morfeldt E, Jonas K, Hultenby K, Ries J, Melefors Ö, Normark S, Henriques-Normark B (2008) Sortase-mediated assembly and surface topology of adhesive pneumococcal pili. Mol Microbiol 70(3):595–607. doi:10.1111/j.1365-2958.2008.06396.x

Gaspar AH, Ton-That H (2006) Assembly of distinct pilus structures on the surface of *Corynebacterium diphtheriae*. J Bacteriol 188(4):1526–1533. doi:10.1128/jb.188.4.1526-1533.2006

Gittes F, Mickey B, Nettleton J, Howard J (1993) Flexural rigidity of microtubules and actin filaments measured from thermal fluctuations in shape. J Cell Biol 120(4):923–934. doi:10.1083/jcb.120.4.923

Guttilla IK, Gaspar AH, Swierczynski A, Swaminathan A, Dwivedi P, Das A, Ton-That H (2009) Acyl enzyme intermediates in sortase-catalyzed pilus morphogenesis in gram-positive bacteria. J Bacteriol 191(18):5603–5612. doi:10.1128/jb.00627-09

Hirata R Jr, Souza SMS, Rocha de Souza CM, Andrade AF, Monteiro-Leal LH, Formiga LCD, Mattos-Guaraldi AL (2004) Patterns of adherence to HEp-2 cells and actin polymerisation by toxigenic *Corynebacterium diphtheriae* strains. Microb Pathog 36(3):125–130. doi:10.1016/j.micpath.2003.10.002

Hirata R Jr, Napoleao F, Monteiro-Leal LH, Andrade AFB, Nagao PE, Formiga LCD, Fonseca LS, Mattos-Guaraldi AL (2002) Intracellular viability of toxigenic *Corynebacterium diphtheriae* strains in Hep-2 cells. FEMS Microbiol Lett 215(1):115–119. doi:10.1111/j.1574-6968.2002.tb11379.x

Hogan M, LeGrange J, Austin B (1983) Dependence of DNA helix flexibility on base composition. Nature 304(5928):752–754. doi:10.1038/304752a0

Huxley HE, Stewart A, Sosa H, Irving T (1994) X-ray diffraction measurements of the extensibility of actin and myosin filaments in contracting muscle. Biophys J 67(6):2411–2421. doi:10.1016/s0006-3495(94)80728-3

Jiao Y, Schäffer TE (2004) Accurate height and volume measurements on soft samples with the atomic force microscope. Langmuir 20(23):10038–10045. doi:10.1021/la048650u

Kang HJ, Paterson NG, Gaspar AH, Ton-That H, Baker EN (2009) The *Corynebacterium diphtheriae* shaft pilin SpaA is built of tandem Ig-like modules with stabilizing isopeptide and disulfide bonds. Proc Natl Acad Sci USA 106(40):16967–16971. doi:10.1073/pnas.0906826106

Koch AL (1966) The logarithm in biology 1. Mechanisms generating the log-normal distribution exactly. J Theoret Biol 12(2):276–290. doi:10.1016/0022-5193(66)90119-6

Kojima H, Ishijima A, Yanagida T (1994) Direct measurement of stiffness of single actin filaments with and without tropomyosin by in vitro nanomanipulation. Proc Natl Acad Sci USA 91(26):12962–12966

Landau LD, Lifshits EM, Pitaevskiĭ LP (1980) Statistical physics. Course of theoretical physics, 3rd edn. Butterworth-Heinemann, Oxford

Landau LD, Lifshitz EM, Kosevich AM, Pitaevskiĭ LP (1986) Theory of elasticity. Course of theoretical physics, 3rd edn. Butterworth-Heinemann, Oxford

Leung KM, Wanger G, Guo Q, Gorby Y, Southam G, Lau WM, Yang J (2011) Bacterial nanowires: conductive as silicon, soft as polymer. Soft Matter 7(14):6617–6621. doi:10.1039/c1sm05611e

Limpert E, Stahel WA (2011) Problems with using the normal distribution—and ways to improve quality and efficiency of data analysis. PLoS ONE 6(7):e21403. doi:10.1371/journal.pone.0021403

Limpert E, Stahel WA, Abbt M (2001) Log-normal distributions across the sciences: keys and clues. Bioscience 51(5):341–352. doi:10.1641/0006-3568(2001)051[0341:LNDATS]2.0.CO;2

Mandlik A, Swierczynski A, Das A, Ton-That H (2007) *Corynebacterium diphtheriae* employs specific minor pilins to target human pharyngeal epithelial cells. Mol Microbiol 64(1):111–124. doi:10.1111/j.1365-2958.2007.05630.x

Mandlik A, Das A, Ton-That H (2008) The molecular switch that activates the cell wall anchoring step of pilus assembly in gram-positive bacteria. Proc Natl Acad Sci USA 105(37):14147–14152. doi:10.1073/pnas.0806350105

Mantelli S, Muller P, Harlepp S, Maaloum M (2011) Conformational analysis and estimation of the persistence length of DNA using atomic force microscopy in solution. Soft Matter 7(7):3412–3416. doi:10.1039/c0sm01160f

Miller E, Garcia T, Hultgren S, Oberhauser AF (2006) The mechanical properties of *E. coli* type 1 pili measured by atomic force microscopy techniques. Biophys J 91(10):3848–3856. doi:10.1529/biophysj.106.088989

Nagashima H, Asakura S (1980) Dark-field light microscopic study of the flexibility of F-actin complexes. J Mol Biol 136(2):169–182

Ott L, Höller M, Rheinlaender J, Schäffer TE, Hensel M, Burkovski A (2010) Strain-specific differences in pili formation and the interaction of *Corynebacterium diphtheriae* with host cells. BMC Microbiol 10:257. doi:10.1186/1471-2180-10-257

Reguera G, McCarthy KD, Mehta T, Nicoll JS, Tuominen MT, Lovley DR (2005) Extracellular electron transfer via microbial nanowires. Nature 435(7045):1098–1101. doi:10.1038/nature03661

Rivetti C, Codeluppi S (2000) Accurate length determination of DNA molecules visualized by atomic force microscopy: evidence for a partial B- to A-form transition on mica. Ultramicroscopy 87(1–2):55–66. doi:10.1016/s0304-3991(00)00064-4

Rivetti C, Guthold M, Bustamante C (1996) Scanning force microscopy of DNA deposited onto mica: Equilibration *versus* kinetic trapping studied by statistical polymer chain analysis. J Mol Biol 264(5):919–932. doi:10.1006/jmbi.1996.0687

Rogers EA, Das A, Ton-That H (2011) Adhesion by pathogenic corynebacteria. In: Linke D, Goldman A (eds) Bacterial adhesion, vol 715. Advances in experimental medicine and biology. Springer, the Netherlands, pp 91–103. doi:10.1007/978-94-007-0940-9_6

Silverman PM, Clarke MB (2010) New insights into F-pilus structure, dynamics, and function. Integr Biol 2(1):25–31. doi:10.1039/b917761b

Skerker JM, Berg HC (2001) Direct observation of extension and retraction of type IV pili. Proc Natl Acad Sci USA 98(12):6901–6904. doi:10.1073/pnas.121171698

Swierczynski A, Ton-That H (2006) Type III pilus of corynebacteria: pilus length is determined by the level of its major pilin subunit. J Bacteriol 188(17):6318–6325. doi:10.1128/jb.00606-06

Taylor WH, Hagerman PJ (1990) Application of the method of phage T4 DNA ligase-catalyzed ring-closure to the study of DNA structure: II. NaCl-dependence of DNA flexibility and helical repeat. J Mol Biol 212(2):363–376. doi:10.1016/0022-2836(90)90131-5

Touhami A, Jericho MH, Boyd JM, Beveridge TJ (2006) Nanoscale characterization and determination of adhesion forces of *Pseudomonas aeruginosa* pili by using atomic force microscopy. J Bacteriol 188(2):370–377. doi:10.1128/jb.188.2.370-377.2006

Trachtenberg S, Hammel I (1992) The rigidity of bacterial flagellar filaments and its relation to filament polymorphism. J Struct Biol 109(1):18–27. doi:10.1016/1047-8477(92)90063-g

Wang MD, Yin H, Landick R, Gelles J, Block SM (1997) Stretching DNA with optical tweezers. Biophys J 72(3):1335–1346. doi:10.1016/s0006-3495(97)78780-0

Wang YA, Yu X, Overman S, Tsuboi M, Thomas GJ Jr, Egelman EH (2006) The structure of a filamentous bacteriophage. J Mol Biol 361(2):209–215. doi:10.1016/j.jmb.2006.06.027

Wright CJ, Shah MK, Powell LC, Armstrong I (2010) Application of AFM from microbial cell to biofilm. Scanning 32(3):134–149. doi:10.1002/sca.20193

Yanagawa R, Honda E (1976) Presence of pili in species of human and animal parasites and pathogens of the genus corynebacterium. Infect Immun 13(4):1293–1295

Yanagida T, Nakase M, Nishiyama K, Oosawa F (1984) Direct observation of motion of single F-actin filaments in the presence of myosin. Nature 307(5946):58–60. doi:10.1038/307058a0